ACS OMEGA

Open Access

http://pubs.acs.org/journal/acsodf

Article

The Leaching Behavior of Potassium Extraction from Polyhalite Ore in Water

Fangtong Ma, Ying Zeng,* Xudong Yu, Ke Chen, and Siying Ren

Cite This: *ACS Omega* 2023, 8, 37162−37175

Read Online

ACCESS | Metrics & More | Article Recommendations

ABSTRACT: The extraction of potassium from polyhalite ore ($K_2SO_4·MgSO_4·2CaSO_4·2H_2O$) can help alleviate potassium resource shortages in China. In this study, the leaching behavior of potassium extracted from polyhalite ore in water was investigated using leaching experiments and kinetic analysis. The effects of various factors, such as liquid-to-solid ratio, leaching temperature, leaching time, and polyhalite ore particle size were comprehensively studied. It was found that high temperatures improved the reaction rate and efficiency at the beginning (1−15 min) but reduced the final leaching efficiency of potassium. And this phenomenon is discussed from the aspects of the dissolution−reprecipitation of potassium, newly formed solid products during the leaching process, and leaching thermodynamics. The leaching of potassium followed the Avrami model, with an apparent activation energy of 26.29 kJ/mol. Additionally, it was determined that the mixed controlled step (surface chemical reaction and diffusion) was the controlling step during potassium leaching. This study clarified the leaching mechanism of the polyhalite in water, and the causes of hindering the leaching of potassium were analyzed. The research results can provide theoretical reference and solutions for parameter design for the enhanced leaching process and selection of leaching agents in the future.

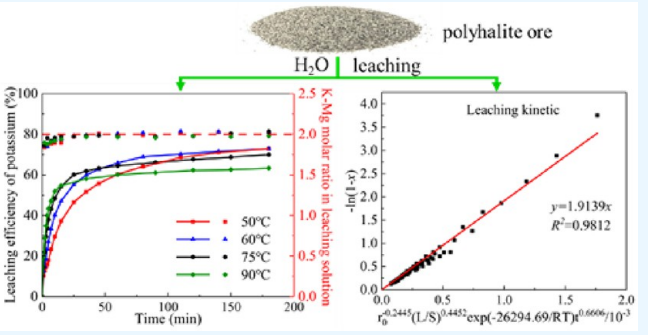

1. INTRODUCTION

Potassium is an essential nutrient for plant growth and plays an irreplaceable role in agricultural production, improving crop yield and quality.[1] China is a large agricultural country, and ensuring food security is a strategic requirement for national development. However, China's external dependence on potassium salt increased approximately 50% in recent years, affecting food security.[2]

Traditionally, potassium is extracted from soluble solid potassium salts such as sylvite and carnallite as well as potassium-rich brines. With the depletion of these resources, there is a growing need to extract potassium from sparingly soluble potassium salts, including potassium feldspar and polyhalite.[3] Polyhalite ($K_2SO_4·MgSO_4·2CaSO_4·2H_2O$) is a promising potassium resource, with a theoretical content of up to 12.966% potassium and large reserves exceeding 10 billion tons when converted to K_2O in the eastern Sichuan Basin.[4]

Polyhalite crystallizes in a triclinic symmetry with the space group $P\bar{1}$ or $F\bar{1}$. The structure consists of [CaO_8] triangular dodecahedra, [MgO_6] octahedra, and [SO_4] tetrahedra with K located in an 11-oxygen-coordinated position.[5,6] The crystal unit cells of polyhalite are shown in Figure 1.[5]

High-grade polyhalite is directly used as a potash fertilizer after being mined and crushed.[7] For low-grade polyhalite resources that can be easily exploited, the roasting−hot leaching method can be used to extract potassium. However, the burial depth of polyhalite resources in the Sichuan Basin is relatively large. The Xuanhan polyhalite deposits, for instance, have a burial depth of more than 3000 m.[4] Therefore, traditional mining technologies are neither technically nor economically viable. In situ leaching mining techniques have matured and increasingly become mature, making it possible to develop and utilize deeply buried polyhalite ores. The leaching performance of polyhalite ore is key to in situ leaching mining technology.

Most previous studies on the leaching of potassium from polyhalite focused on screening leaching agents.[8] Organic acids and inorganic salts are commonly used reagents for the leaching of polyhalite ores. Common organic acids include formic and oxalic acids. The results indicate that organic acids facilitate the leaching of K^+ and Mg^{2+}. However, one of the biggest issues with organic acid leaching is serious environmental pollution. For inorganic salt leaching agents, there is a general rule that the leaching effect of polyhalite under the same solvent varies greatly due to the mineralogical characteristics of polyhalite. For

Received: July 3, 2023
Accepted: September 15, 2023
Published: September 28, 2023

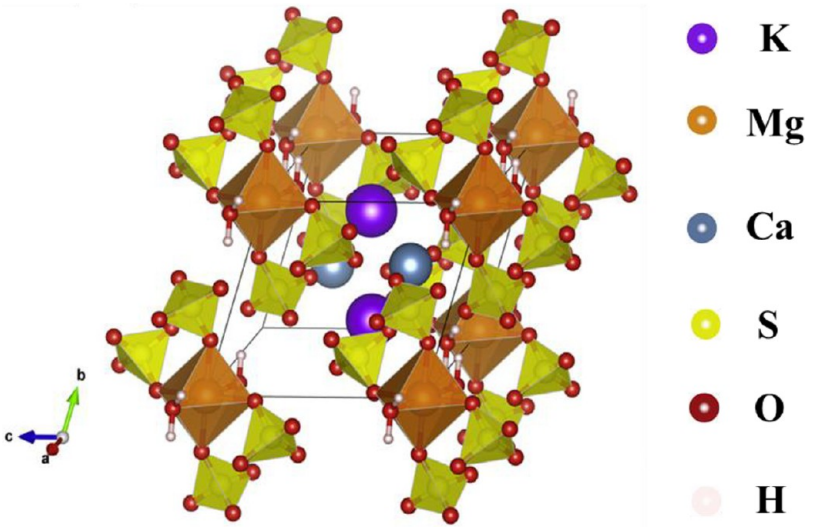

Figure 1. Crystal unit cells of polyhalite ($K_2SO_4{\cdot}MgSO_4{\cdot}2CaSO_4{\cdot}2H_2O$).

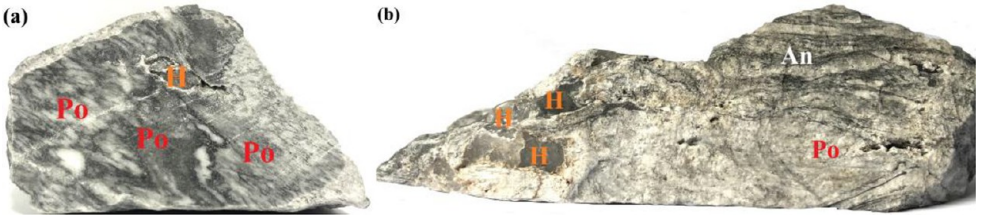

Figure 2. Photos of the polyhalite potassium ore in Chuan Xuan Di No. One well (a) at 3149 m and (b) at 3051 m. An, anhydrite; Po, polyhalite; H, halite.

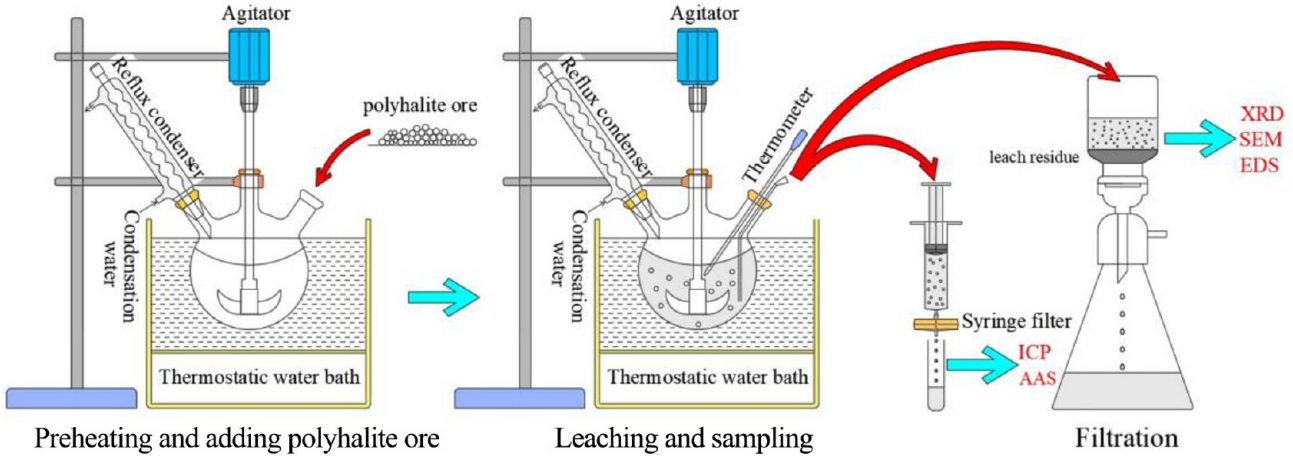

Figure 3. Schematic diagram of the leaching instrument and polyhalite ore leaching process.

example, NaCl solution and $Ca(OH)_2$ solution have good solubilization effects on Quxian polyhalite. However, the leaching effect of potassium from Kunteyi salt lake polyhalite in NaCl solution and $Ca(OH)_2$ solution is not as good as that of H_2O.[9]

Currently, the research on the leaching behavior of polyhalite in Xuanhan is not thorough or systematic, and the leaching mechanism remains unclear. Whether this type of polyhalite ore has good leaching performance depends on either the thermodynamic stability or the formation of calcium sulfate inclusions during the leaching process.

This study systematically investigated the effects of stirring speed, liquid-to-solid ratio, leaching temperature, leaching time, and polyhalite ore particle size on the potassium leaching efficiency, and the leaching kinetics of potassium were analyzed. The study determined the factors that affect the leaching rate and the control steps of the leaching process. These findings provide a basis for improving the process of potassium leaching from polyhalite.

2. MATERIALS AND EXPERIMENTS

2.1. Materials and Reagents. The polyhalite ore sample used in this study was obtained from Xuanhan, Sichuan Province, China, and its appearance is shown in Figure 2. The sample was primarily composed of polyhalite, with a few massive halites and banded anhydrites distributed throughout. To

https://doi.org/10.1021/acsomega.3c04733
ACS Omega 2023, 8, 37162−37175

Table 1. XRF Results of Polyhalite Ore (wt %)

Particle size (μm)	K_2O	MgO	CaO	SO_3	Na_2O	SiO_2	SrO	Cl	Al_2O_3
−450 + 300	13.10	8.29	17.29	50.20	0.88	0.99	0.31	0.89	0.10
−170 + 125	13.37	7.78	18.15	50.62	0.69	0.69	0.32	0.63	0.07
−125 + 98	13.45	7.76	17.90	51.10	0.52	0.64	0.33	0.58	0.06
−88 + 63	13.33	8.02	17.48	50.15	0.58	0.98	0.32	0.58	0.09

prepare for a series of leaching experiments, the polyhalite ore was ground using a pulverizer and then sieved to obtain different particle size fractions (−450 + 300 μm, −170 + 125 μm, −125 + 98 μm and −88 + 63 μm). Deionized water was used in all experiments.

2.2. Leaching Experiment. The leaching reaction was carried out in a 250 mL three-necked flask heated in a thermostatic water bath to minimize experimental error. A total of 120 mL of water at the selected temperature was placed in the flask. Subsequently, the reactor was heated to a specific temperature before the sample was added. At predetermined time intervals, an aliquot of the solution was quickly removed and filtered using 0.22 μm syringe filters. The concentrations of potassium, magnesium, and calcium in the leaching solution were measured by using inductively coupled plasma optical emission spectrometry (ICP-OES) and atomic absorption spectroscopy (AAS). Section 3.2.3 was researched in parallel three times to ensure its reliability. Figure 3 shows a schematic of the leaching instrument and the polyhalite ore leaching process.

The leaching efficiency of potassium and magnesium were calculated using the following expression:

$$x = \frac{v \cdot c}{m \cdot w} \quad (1)$$

where c is the concentration of potassium in the leaching solution, v is the volume of the leaching solution, m is the mass of the added polyhalite ore, and w is the mass fraction of potassium in the polyhalite ore.

2.3. Analytical Methods. X-ray fluorescence spectrometry (XRF; Zetium, PANalytical, Netherlands) was used to determine the composition of polyhalite ore. The mineral phase compositions of the polyhalite ore and the leaching residues were detected using X-ray diffraction (XRD, Ultima IV, Rigaku, Japan) using Cu Kα radiation with the testing angle ranging from 10° to 60° at a scanning rate of 15°/min. The microstructural and elemental distribution of the leaching residues were detected and scanned using a scanning electron microscope (SEM; Sigma 300, ZEISS, Germany; Inspect F50, FEI, USA) equipped with a backscattered electron (BSE) and an energy dispersive spectrometer (EDS; OXFORD, UK). The particle size distribution of the polyhalite ore was analyzed by using a laser particle size analyzer (Mastersizer 2000, Malvern, Britain). The potassium, magnesium, and calcium contents of the polyhalite ore and leachates were determined using inductively coupled plasma optical emission spectrometry (ICP-OES, Avio 200, PerkinElmer, USA) and atomic absorption spectroscopy (AAS, ICE-3300, Thermo Fisher Scientific, USA).

3. RESULTS AND DISCUSSION

3.1. Mineralogical Characteristics. In this study, mineralogical analyses of ore samples are carried out using XRF, ICP-OES, AAS, XRD, BSE, and EDS to determine the main constituents and content of ore samples.

The chemical compositions of the ore samples were analyzed using an X-ray fluorescence spectrometer (XRF) and are given in Table 1. As shown, the polyhalite ore was primarily composed of K_2O, MgO, CaO, and SO_3, accounting for more than 13%, 7.7%, 17%, and 50% of the ore, respectively. Na_2O, SiO_2, SrO_2, Cl, and Al_2O_3 were present in contents of less than 1% in all particle sizes.

The potassium, magnesium, and calcium contents of the polyhalite ore were determined using inductively coupled plasma optical emission spectrometry (ICP-OES) and atomic absorption spectroscopy (AAS), and the K−Mg−Ca molar ratio was calculated. The results are summarized in Table 2.

Table 2. Contents of K, Mg, and Ca in the Polyhalite Ore (wt %) and K−Mg−Ca Molar Ratio

Particle size (μm)	K	Mg	Ca	K−Mg−Ca molar ratio
−450 + 300	12.31	4.43	13.32	2:1.16:2.16
−170 + 125	12.60	4.38	13.35	2:1.12:2.12
−125 + 98	12.49	4.32	13.81	2:1.11:2.21
−88 + 63	12.35	4.28	13.65	2:1.11:2.21
Theoretical values	12.97	4.03	13.29	2:1:2

The chemical composition of the polyhalite ore was analyzed using X-ray diffraction (XRD), and the results are shown in Figure 4. The results indicate that the ore sample was mainly composed of polyhalite. The diffraction peaks of other minerals that are not visible may be due to the low content.

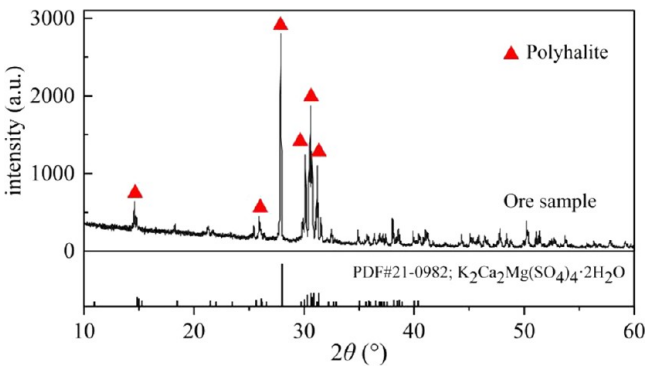

Figure 4. XRD pattern of the polyhalite ore.

The morphology and elemental distribution of the polyhalite ore were determined by using backscattered electron (BSE) and energy dispersive spectrometry (EDS). The BSE images and related EDS results for the polyhalite ore are shown in Figure 5 and Table 3.

Three different minerals were found to be present in the particles, as shown in Figure 5b. Based on EDS (Table 3) results, the dark black part of position 1 in Figure 5b is the major composition likely being periclase and dolomite. The major composition of the dark gray part at position 2 in Figure 5b was confirmed to be polyhalite. The major composition of the bright

https://doi.org/10.1021/acsomega.3c04733
ACS Omega 2023, 8, 37162−37175

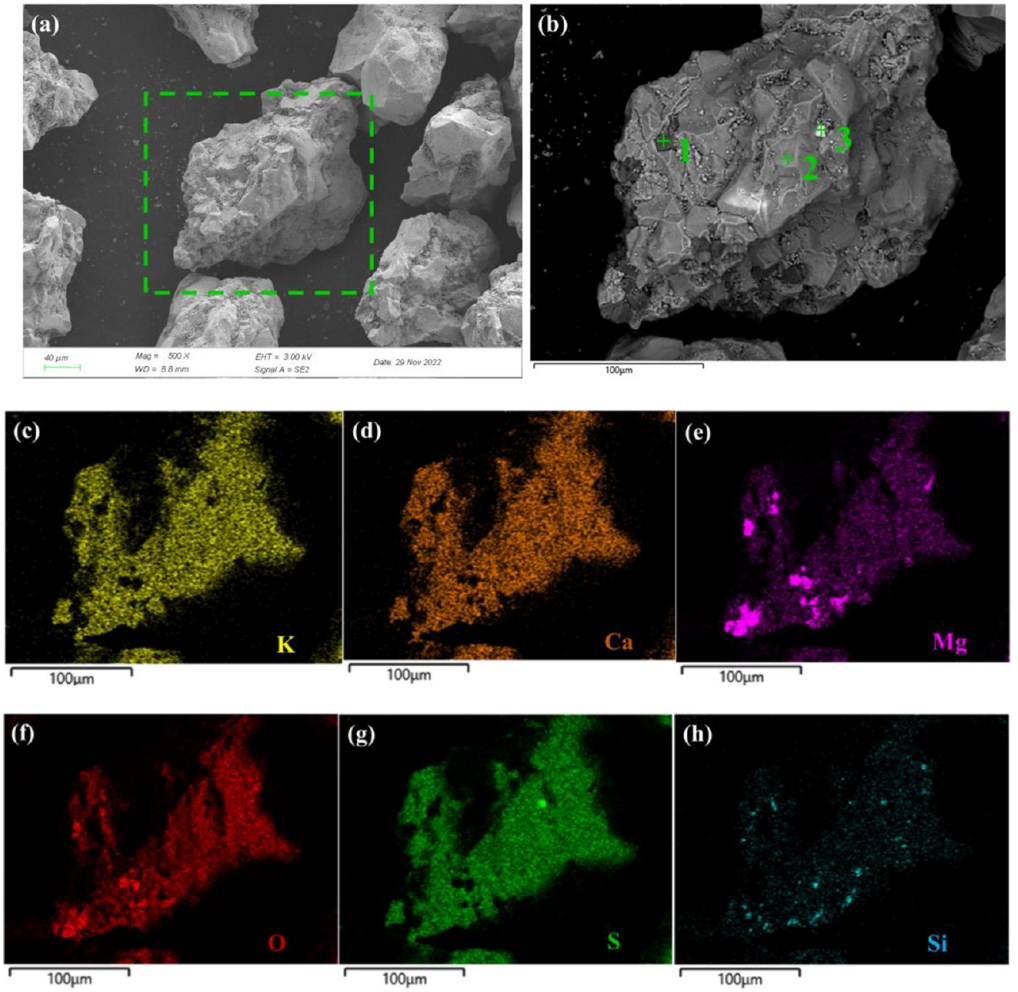

Figure 5. BSE images (a, b) and elemental mappings (c–h) of polyhalite ore.

Table 3. EDS Analysis Results

	Elements (wt %)							
Position in Figure 5	K	Ca	Mg	S	O	Si	Fe	Main minerals
1	0.32	–	38.65	0.49	60.34	0.21	–	Periclase or Dolomite
2	9.66	14.32	4.76	23.05	48.21	–	–	Polyhalite
3	–	–	0.46	44.44	4.99	0.44	49.67	Pyrite
Mapping	11.13	11.22	5.59	18.70	52.70	0.47	–	Polyhalite

white part of position 3 in Figure 5b is likely pyrite. Elemental mapping of the polyhalite ore surface in Figure 5c–h revealed large amounts of K, Mg, Ca, and S, with sporadic Si. In addition, K, Mg, Ca, O, and S were uniformly distributed and have good relevance, and the mass percentages of K, Mg, Ca, O, and S (Table 3) were similar to those of polyhalite, indicating that this mineral is polyhalite.

By combining the data in Table 1, Table 2, Figure 4, Figure 5, and Table 3, we can confirm that the ore sample is a high-purity polyhalite ore, possibly containing small amounts of anhydrite, halite, periclase, dolomite, pyrite, and silicates.

3.2. Effect of Reaction Conditions on the Potassium Extraction Efficiency. *3.2.1. Effect of Stirring Speed.* The leaching mechanism of polyhalite in water is a typical solid–liquid two-phase reaction. The flow field environment affects the heat–mass transfer of the solution reaction. Mechanical stirring can reflect flow patterns, velocity distribution, and other flow field characteristics. Therefore, the influence of the flow field characteristics on the leaching of polyhalite was investigated through mechanical agitation.

The effects of stirring speed on potassium leaching efficiency were investigated at stirring speeds of 250, 350, 450, and 550 r/min, while other leaching parameters were maintained at a leaching temperature of 90 °C, a particle size of −170 + 125 μm, and a liquid-to-solid ratio of 10:1 mL/g. The results are presented in Figure 6.

According to Figure 6, with an increase in stirring speed from 250 to 450 r/min, the leaching efficiencies of K increased from 46.54% to 51.92% when the leaching time exceeded 10 min. This is because increasing the stirring speed suspended the solid particles in the solution, enabling better contact between the leaching solution and the particles. Additionally, a higher stirring speed can reduce the thickness of the diffusion layer formed

https://doi.org/10.1021/acsomega.3c04733
ACS Omega 2023, 8, 37162–37175

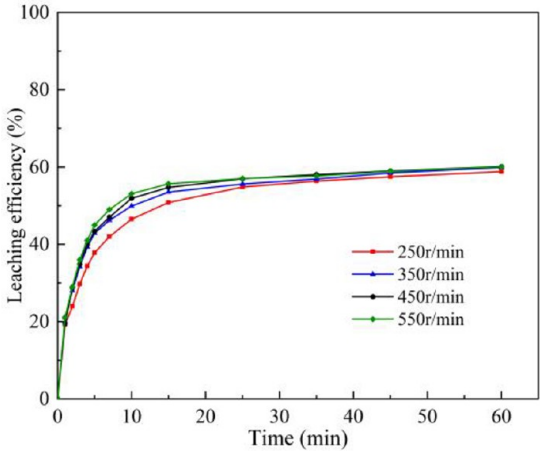

Figure 6. Effect of stirring speed on leaching efficiency of potassium from polyhalite ore in water.

around the particles, accelerating the mass transfer and external diffusion of the reactants.[10]

When the stirring speed was higher than 450 r/min, there was no significant improvement in potassium leaching. This is because the solid particles were fully suspended in the solution, and increasing the stirring speed no longer reduced the thickness of the mass transfer boundary layer, indicating that the effects of external diffusion and external mass transfer became negligible. Therefore, all subsequent experiments were conducted at 450 r/min to investigate the effects of other leaching factors.

3.2.2. Effect of Liquid-to-Solid Ratio. The liquid-to-solid ratio had a considerable influence on the polyhalite extraction efficiency and concentration of K^+ after leaching. The effects of liquid-to-solid ratio on the leaching of polyhalite minerals were examined at liquid-to-solid ratios of 6, 10, 14, and 18 mL/g. These experiments kept the stirring speed, temperature, and particle size constant at 450 r/min, 60 °C, and −170 + 125 μm, respectively. The results are listed in Figure 7.

As shown in Figure 7a, when the liquid-to-solid ratio increased from 6:1 to 18:1 mL/g, the potassium leaching efficiency increased sharply from 48.69% to 99.99% in 180 min. The liquid−solid ratio mainly affected leaching in two ways. First, increasing the liquid−solid ratio can increase the relative amounts of the leaching agent to solids, increase the contact surface between particles and leaching agent, thus increasing the leaching efficiency.[11] Second, increasing the liquid−solid ratio also reduces the viscosity and improves the fluidity and diffusion of the reaction system, which improves the mass transfer of the leaching reaction.[12] Moreover, when the liquid-to-solid ratio decreases, the concentration of insoluble products increases correspondingly, which may cover the ore surface, preventing the leaching reaction and thus decreasing the leaching efficiency of potassium.

Figure 7b shows the concentration of potassium in leaching solution under different liquid−solid ratios and leaching times. However, this is contrary to the leaching efficiency of potassium, where the concentration of potassium in leaching solution decreases from 10.24 g/L to 7.01 g/L with liquid−solid ratio increasing from 6:1 mL/g to 18:1 mL/g at 180 min. Although a high liquid-to-solid ratio can result in a high potassium extraction efficiency, the potassium solution formed has a low concentration, making it difficult to utilize further. Therefore, a balance between leaching efficiency and concentration is necessary when determining the optimal liquid−solid ratio.

3.2.3. Effect of Reaction Temperature and Time. The effect of temperature and time on the dissolution of potassium from the polyhalite ore was investigated at 50 °C, 60 °C, 75 °C, and 90 °C, respectively, based on the geothermal temperature of polyhalite ore layers. While other leaching parameters were maintained at a stirring speed of 450 rpm, a liquid-to-solid ratio of 10:1 mL/g, and a particle size of −170 + 125 μm.

The leaching efficiencies of potassium and magnesium at different temperatures are shown in Figure 8 and Figure 9. The K−Mg molar ratios in the leaching solution at different temperatures are shown in Figure 9. The calcium concentrations at different temperatures are listed in Figure 10.

As shown in Figure 8, the temperature strongly influences potassium leaching efficiency. The leaching efficiency of K increases rapidly at the beginning of the leaching process. When the reaction time is 10 min, the leaching efficiencies of potassium are 29.54%, 40.18%, 48.44%, and 51.92% at the temperatures of 50 °C, 60 °C, 75 and 90 °C, respectively. Moreover, the higher the temperature, the higher the leaching efficiency of potassium in 1−15 min. This is because increasing the temperature decreases the viscosity of the reaction medium and accelerates diffusion and mass transfer, which can promote water from the surface to enter the interior of the ore particles, accelerating the decomposition of the polyhalite ore. Moreover, the average kinetic energy of the molecules increases with an increase in the

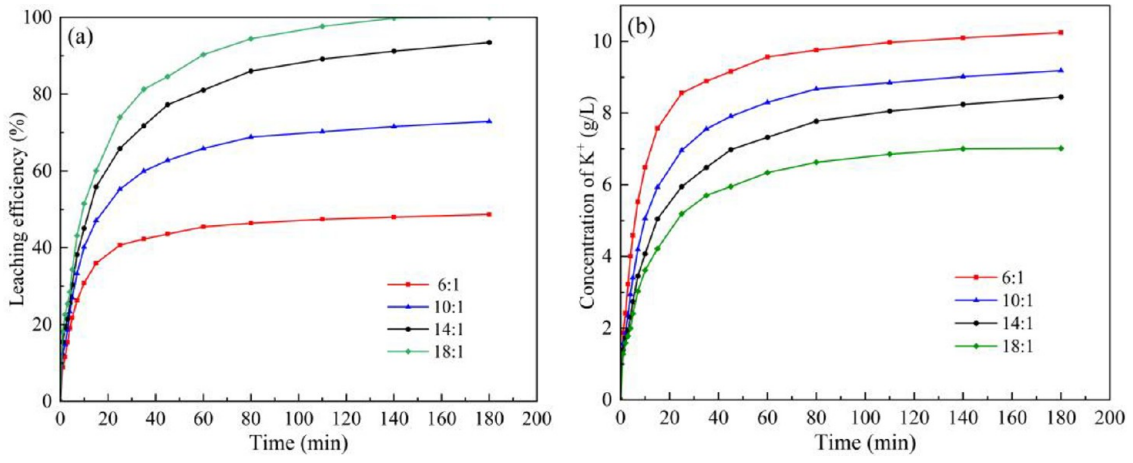

Figure 7. Effect of liquid−solid ratio on leaching efficiency of potassium (a) and potassium ion concentration (b) in the leaching solution.

https://doi.org/10.1021/acsomega.3c04733
ACS Omega 2023, 8, 37162−37175

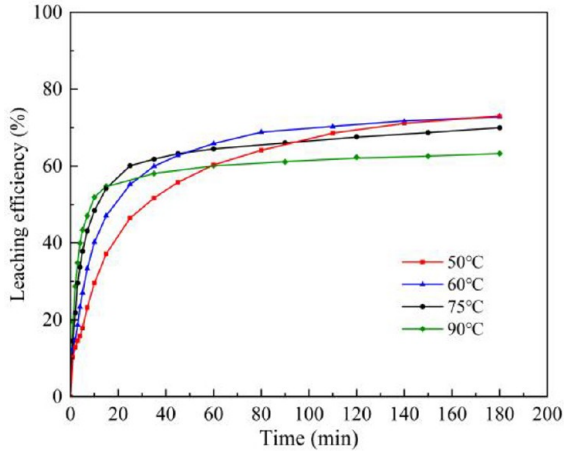

Figure 8. Effect of the reaction temperature and time on the leaching efficiency of potassium.

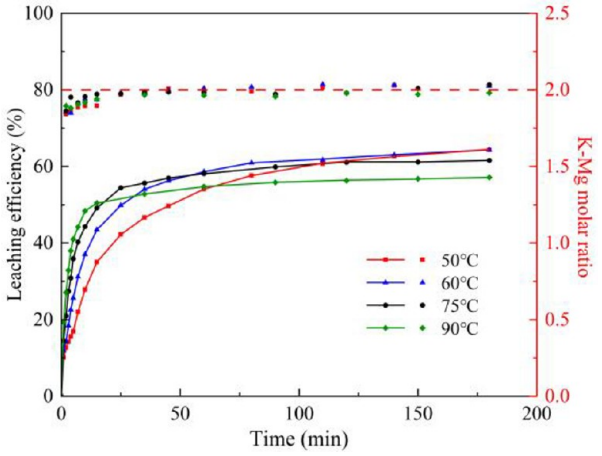

Figure 9. Effect of reaction temperature on leaching efficiency of magnesium and K−Mg molar ratio in leaching solution.

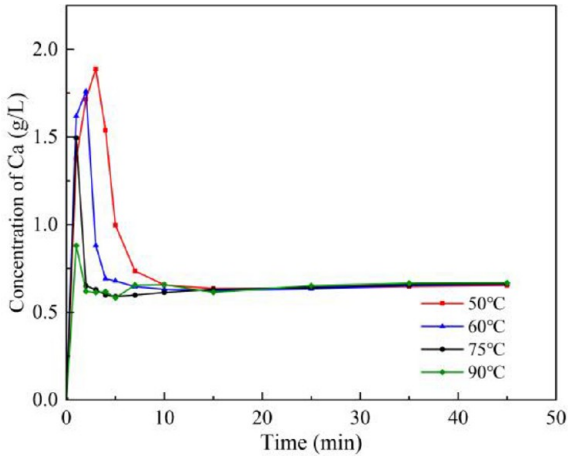

Figure 10. Effect of the reaction temperature and time on the concentration of Ca in the leaching solution.

leaching temperature, causing more frequent and stronger collisions between the molecules, and hence increasing the reaction rate.[13]

However, when the leaching time exceeds 15 min, the leaching efficiency of potassium at 75 °C, 60 °C, and 50 °C gradually exceeds 90 °C with further prolonging of the reaction time. The leaching efficiency of potassium decreases from 72.90% to 63.27% at 180 min, as the reaction temperature increases from 50 to 90 °C. The results show that higher temperatures suppress the leaching efficiency of K in the later stages of the leaching reaction, which is an interesting phenomenon. And this phenomenon is discussed from the aspects of the dissolution-reprecipitation of potassium, newly formed solid products during the leaching process, and leaching thermodynamics.

As shown in Figure 8 and Figure 9, Mg is in good agreement with the change trends of the K leaching efficiency vs temperature and time. The K−Mg molar ratio in the leaching solution was almost equal to 2, which is consistent with the theoretical molar ratio of potassium and magnesium in polyhalite. Additionally, no newly formed K-bearing minerals were significantly found in the leaching residue (and will be discussed in more detail in Section 3.3.1), indicating that the potassium ions released from polyhalite dissolution in water do not form secondary potassium bearing minerals (e.g., K_2SO_4, $K_2Ca_5(SO_4)_2{\cdot}H_2O$, $K_2Ca_5(SO_4)_6{\cdot}H_2O$, $K_2Mg_2(SO_4)_3$, $K_2Mg(SO_4)_2{\cdot}4H_2O$, $K_2Mg(SO_4)_2{\cdot}6H_2O$). This excluded the possibility that the low leaching rate of potassium due to K-bearing precipitates production at high temperatures in the later stages of the leaching reaction.

As shown in Figure 10, the concentration of calcium in the leaching solution first increased and then decreased with an increasing leaching time. This is attributed to calcium ions reacting with sulfate ions to form calcium sulfate. Furthermore, at the beginning of the reaction, the higher the temperature, the lower the calcium ion concentration. Increasing the temperature will shorten the "induction period" of calcium sulfate at the initial crystallization stage, thereby accelerating the crystal nucleation rate.[14] Moreover, as shown in Figure 14b−d, the particle size of the leaching product decreases with an increase in the leaching temperature, which leads to an increase in the viscosity of the system and hinders the mass transfer and diffusion of reactants during the leaching process. This may also be one of the reasons for the low leaching efficiency of potassium.

To further explore the influence of temperature, the thermodynamic parameters of Gibbs free energies (ΔG) and reaction equilibrium constants (Log K) of the polyhalite dissolution process (eq 2) were calculated by eqs 3−7,[15] while thermodynamic data of reactants and products can be acquired from related literature (Table 4),[16−18] and the results are shown in Figure 11.The major mineral compositions of leaching residues are $CaSO_4{\cdot}2H_2O$. Thus, it is deduced that there exist chemical equations in polyhalite leaching with water as follows:

$$K_2SO_4{\cdot}MgSO_4{\cdot}2CaSO_4{\cdot}2H_2O + 2H_2O \rightarrow 2K^+ + Mg^{2+} + 2SO_4^{2-} + 2CaSO_4{\cdot}2H_2O \quad (2)$$

$$\Delta_r H_m^\theta = \sum \nu_B \Delta_f H_m^\theta(P) - \sum \nu_B \Delta_f H_m^\theta(R) \quad (3)$$

$$\Delta_r S_m^\theta = \sum \nu_B \Delta_f S_m^\theta(P) - \sum \nu_B \Delta_f S_m^\theta(R) \quad (4)$$

$$\Delta_r G_m^\theta = \sum \nu_B \Delta_f G_m^\theta(P) - \sum \nu_B \Delta_f G_m^\theta(R) \quad (5)$$

$$\Delta G = \Delta H - T\Delta S \quad (6)$$

$$\Delta G = -RT \ln K \quad (7)$$

https://doi.org/10.1021/acsomega.3c04733
ACS Omega 2023, 8, 37162−37175

Table 4. Thermodynamic Data of Reactants and Products

Substance	$\Delta_f H_m^\theta$(298.15 K) (kJ·mol^{-1})	$\Delta_f G_m^\theta$(298.15 K) (kJ·mol^{-1})	ΔS_m^θ(298.15 K) (J·K^{-1}·mol^{-1})
$K_2SO_4·MgSO_4·2CaSO_4·2H_2O$ (cr)[16]	−6121 ± 21	−559 ± 21	599.1 ± 1.3
$CaSO_4·2H_2O$ (cr)[17,18]	−2022.63	−1797.28	194.10
H_2O(l)[17,18]	−285.83	−237.129	69.91
Ca^{2+}(aq)[17,18]	−542.83	−553.58	−53.10
K^+(aq)[17,18]	−252.38	−283.27	102.50
Mg^{2+}(aq)[17,18]	−466.85	−454.80	−138.10
SO_4^{2-}(aq)[17,18]	−909.27	−744.53	20.10

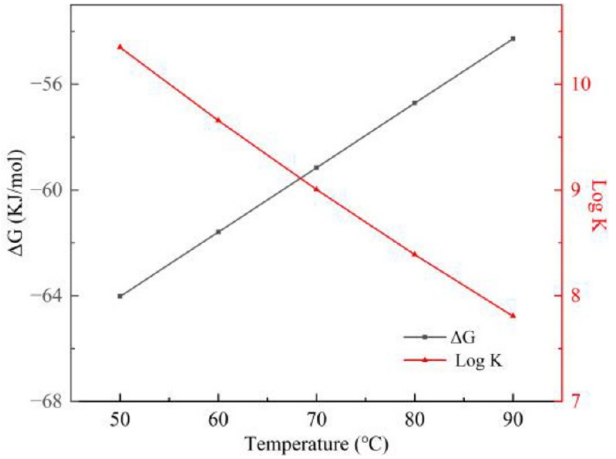

Figure 11. Relationship between ΔG, Log K, and temperature for the possible reactions during polyhalite leaching with water.

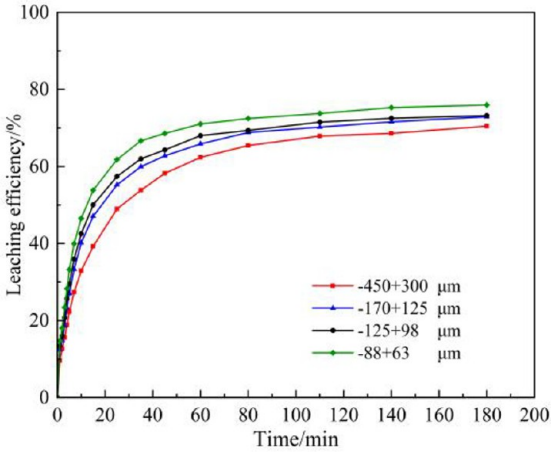

Figure 12. Effect of particle size on leaching efficiency of potassium from polyhalite ore in water.

where ΔH is the enthalpy change, kJ·mol^{-1}; ΔS is the entropic change, J·K^{-1}·mol^{-1}; ΔG is the Gibbs free energy, kJ·mol^{-1}; v is the stoichiometric number; T is the reaction temperature, K; R is the mole gas constant, 8.314 J·K^{-1}·mol^{-1}; K is the equilibrium constant.

According to Figure 11, within the temperature range of 50−90 °C, the ΔG of reaction 2 increases with increasing temperature, and the equilibrium constant Log K decreases with increasing temperature. Generally, the more negative the ΔG value and the more positive the Log K value of the leaching reaction, the greater the forward trend of the reaction.[15,19,20] This implies that increasing the reaction temperature thermodynamically reduces the driving force of the chemical reaction, thus weakening the forward trend of the polyhalite leaching reaction. Therefore, the variation of experimental results with temperature is consistent with the thermodynamic trend.

Furthermore, an increase in temperature leads to a significant expansion of the polyhalite formation region in the phase diagram of six-component system Na^+, K^+, Mg^{2+}, Ca^{2+}//Cl^-, SO_4^{2-}−H_2O at 15−83 °C.[21] Additionally, the analysis of this phenomenon from a phase chemical point of view indicates that an increase in temperature leads to a decrease in the solubility of polyhalite.

3.2.4. Effect of Particle Size. To examine the effect of particle size on the leaching of polyhalite mineral, the experiments were carried out using the ore with particle sizes of −450 + 300 μm, −170 + 125 μm, −125 + 98 μm, and −88 + 63 μm, while the stirring speed, solid-to-liquid ratio, and temperature were kept constant at 450 r/min, 10 mL/g, and 60 °C, and the results are shown in Figure 12.

As shown in Figure 12, the smaller the particle size, the higher the leaching efficiency and the faster the leaching of polyhalite. This is because with a decrease in particle size the specific surface area increases, the contact surface between the solid and liquid reactants grows, and the internal diffusion resistance decreases.

3.3. Characterization of Leaching Residue. To understand the structural evolution and mechanism of the leaching process, the morphologies of the leaching residues were analyzed by using XRD, BSE, and EDS.

3.3.1. XRD Analysis of the Leach Residue. The leaching residue was analyzed by using XRD to determine the phase composition of the leaching product.

Figure 13 indicates that all major diffraction peaks of the raw ore could be assigned to polyhalite, the diffraction peaks of polyhalite in leach residues significantly weakened, indicating that most of the polyhalite was dissolved in water after leaching. Meanwhile, new evident peaks are detected at 11.69°, 20.76°, 23.44°, and 29.14° in the XRD pattern of the leaching residue, which belongs to gypsum ($CaSO_4·2H_2O$). Compared with polyhalite, the characteristic peaks of gypsum were most prominent, indicating that gypsum is the primary component of residues. Additionally, no characteristic peaks of newly K-bearing minerals were significantly found in the leaching residue, indicating that the potassium ions released from polyhalite dissolution in water do not form secondary potassium bearing minerals.

3.3.2. BSE and EDS Analysis. Based on the XRD analysis results of the leaching residue, it was found that the solid product $CaSO_4·2H_2O$ is produced during the leaching of polyhalite. The morphology of $CaSO_4·2H_2O$, whether it is precipitated and coated on the surface of unreacted polyhalite, and the compactness of the coating all have important effects on the leaching behavior of polyhalite.

https://doi.org/10.1021/acsomega.3c04733
ACS Omega 2023, 8, 37162−37175

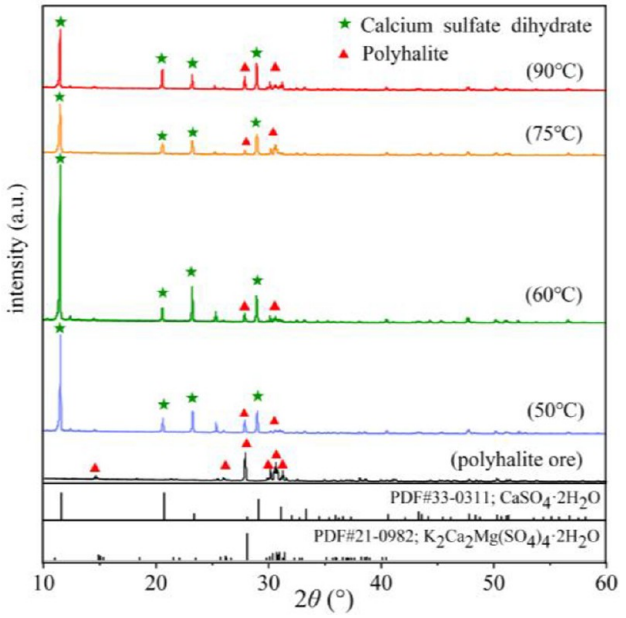

Figure 13. Comparison of XRD patterns of the residues at various reaction temperatures: 50 °C, 60 °C, 75 °C, and 90 °C.

Therefore, the morphologies of the leaching residues at different temperatures were analyzed using BSE, and the results are presented in Figure 14.

As shown in Figure 14, the particle size of the polyhalite ore in the residue decreases slightly, and a considerable number of $CaSO_4{\cdot}2H_2O$ crystals were observed. The crystal morphology of $CaSO_4{\cdot}2H_2O$ in the leach residue is mainly a sheet at the temperatures of 50 °C. The sheet morphology of $CaSO_4{\cdot}2H_2O$ gradually transformed to a columnar or needle-like morphology with increasing temperature. A decrease in the particle size of $CaSO_4{\cdot}2H_2O$ leads to an increase in the viscosity of the leaching system, which may increase the mass transfer resistance and hinder the reaction, and this is consistent with the results in Figure 8.

To further explore whether $CaSO_4{\cdot}2H_2O$ precipitated and coated on the surface of unreacted polyhalite and the compactness of the coating, BSE-EDS-Mapping analysis was used to further identify the elemental distribution of the unreacted polyhalite particles. The results are presented in Figure 15 and Table 5.

As shown in Figure 15 and Table 5, most of the calcium was precipitated as $CaSO_4{\cdot}2H_2O$ during the leaching of polyhalite, and a portion of $CaSO_4{\cdot}2H_2O$ covered some areas (e.g., positions 2 and 5) on the surfaces of the unreacted polyhalite particles and then blocked the reaction between water and polyhalite ore to a certain extent. The mass percentages of K, Mg, Ca, O, and S at position 6 (Figure 15b) were similar to those of polyhalite, indicating that $CaSO_4{\cdot}2H_2O$ crystals did not cover the regions. A small amount of potassium was detected in some regions (e.g., position 3 and position 4), and the mass percentages of K on the surface of the leaching residues are much smaller than those of the raw ores, indicating the presence of coating on the regions but not dense, which can be further confirmed by the element distribution images of the leaching residues (Figure 15e–j). Because the polyhalite particles could not be thoroughly coated, some areas of the polyhalite particles could still establish effective contact with the leaching agent.

3.4. Leaching Kinetics of Potassium and Magnesium from Polyhalite. To obtain a better understanding of the mechanisms of potassium leaching from polyhalite ore in water, leaching kinetic analysis was employed to explore the chemical behaviors occurring during the leaching reaction.

3.4.1. Kinetic Model. The leaching of polyhalite ore in water is a typical solid–liquid two-phase reaction. Generally, the rate of mineral leaching can be controlled by diffusion through a fluid film, diffusion through an ash or product layer, or surface chemical reactions. Because the leaching reaction proceeds under mechanical stirring, the diffusion resistance through the liquid film should be negligible. Furthermore, solid product of $CaSO_4{\cdot}2H_2O$ formed on the surface of unreacted polyhalite particles during leaching according to XRD, BSE, and EDS analysis results (Figure 13, Figure 15, and Table 5). Because the $CaSO_4{\cdot}2H_2O$ wrapped on the surface of unreacted polyhalite particles hinders the contact between the leaching solution and unreacted polyhalite, controlled diffusion through an ash or product layer may become a control step. Combined with the selection the basis of kinetic models, the reaction kinetics of polyhalites can be interpreted using shrinking core models and the Avrami model.[22,23]

Surface chemical reaction- and diffusion-controlled processes can be applied to describe the kinetics of the polyhalite leaching process, which can be expressed as follows:

$$1 - (1 - x)^{1/3} = k_1 t \quad \text{(surface chemical reaction-controlled)} \tag{8}$$

$$1 - \frac{2}{3}x - (1 - x)^{2/3} = k_2 t \quad \text{(product-layer diffusion-controlled)} \tag{9}$$

where x is the potassium leaching efficiency, t is the leaching time (min), and k_1 and k_2 are the apparent rate constants determined using eqs 8 and 9, respectively.

The results of $1 - (1 - x)^{1/3}$ and $1 - 2x/3 - (1 - x)^{2/3}$ versus time t at different temperatures are shown in Figure 16a,b, respectively.

As shown in Figure 16, the kinetic data of potassium fit poorly to the surface chemical reaction control model and the product layer diffusion control model ($R^2 < 0.99$). Therefore, the kinetics of potassium leaching from the polyhalite ore in water cannot be analyzed using a surface chemical reaction control model or product layer diffusion control model.

The Avrami model was initially developed to describe crystallization kinetics.[24,25] The leaching reaction can be regarded as the reverse of the crystallization process. Thus, the Avrami model can also be used to explain the kinetics of the crystal leaching reaction.[23]

The Avrami model successfully described the leaching kinetics of various solid–liquid reactions.[26] The kinetic equation of the Avrami model is given as

$$-\ln(1 - x) = kt^n \tag{10}$$

The logarithm is taken on both sides of eq 10 to obtain eq 11.

$$\ln[-\ln(1 - x)] = \ln k + n \ln t \tag{11}$$

where x is the leaching efficiency of potassium, k is the apparent reaction efficiency constant of the leaching process, t is the leaching time, and n is the characteristic constant. When $n < 0.5$, the Avrami equation is diffusion-controlled; when $0.5 \leq n < 1$,

https://doi.org/10.1021/acsomega.3c04733
ACS Omega 2023, 8, 37162–37175

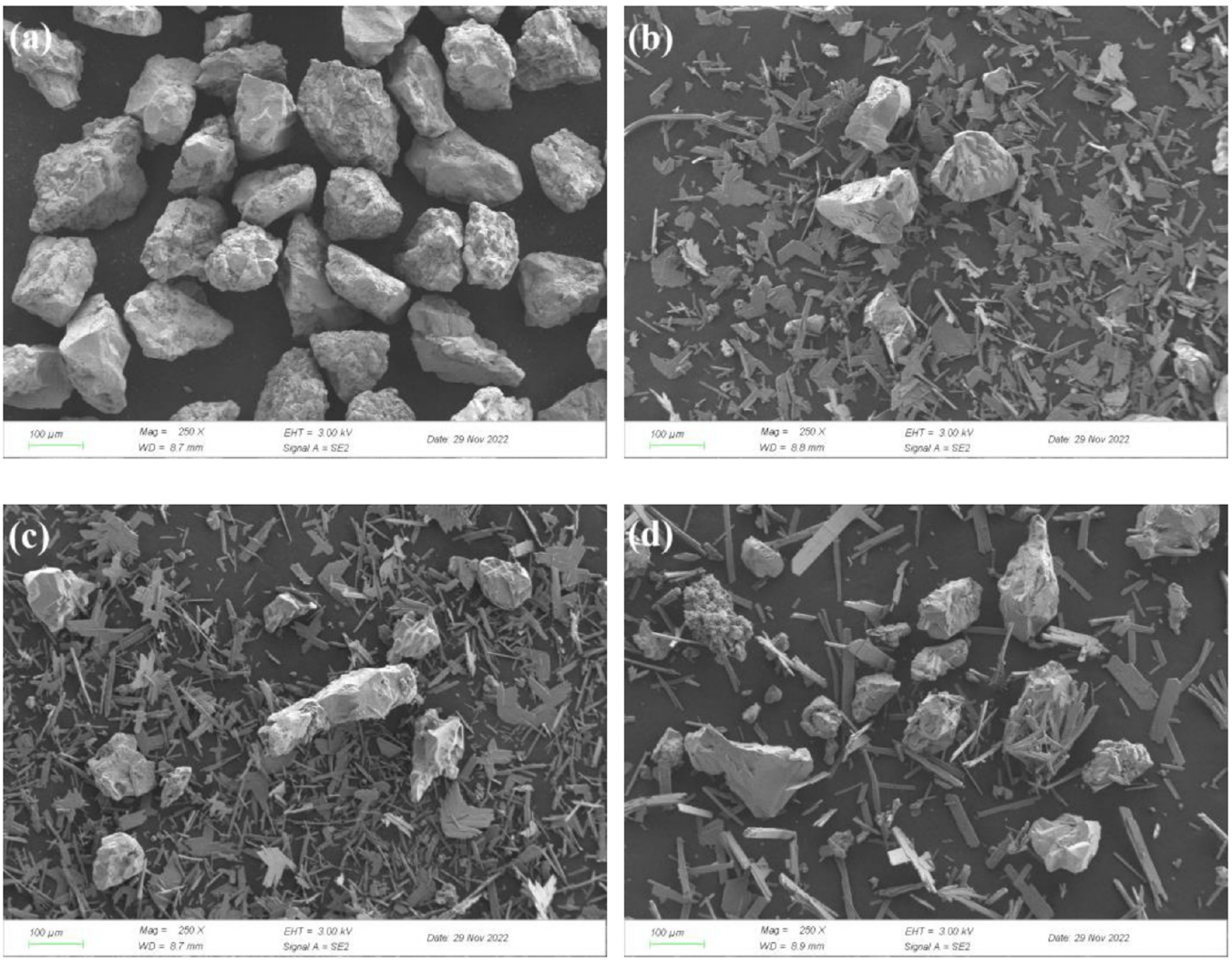

Figure 14. BSE images of polyhalite ore and the leach residue: (a) polyhalite ore; (b) residue (50 °C); (c) residue (75 °C); (d) residue (90 °C) (Reaction time: 180 min, Particle size: −170 + 125 μm, L/S:10:1 mL/g, Stirring speed: 450 r/min).

the leaching process is a mixed type of chemical reaction and diffusion control.[27]

The plots of $\ln[-\ln(1-x)]$ versus $\ln t$ at different temperatures for potassium leaching are presented in Figure 17.

As shown in Figure 17, the correlation coefficient R^2 of the Avrami model is greater than 0.99, indicating that the models fit the data well in the leaching experiments. Furthermore, the n values obtained using the Avrami equation at different temperatures were all between 0.5−1, and the leaching process was a mixed type of chemical reaction and diffusion control.

3.4.2. Calculation of the Activation Energy. The apparent activation energy is an important feature used to describe the control of the leaching kinetics. Chemical bonds are destroyed during a chemical reaction; thus, the activation energy of the chemical-reaction-controlled process is typically higher than that of the diffusion controlled process. The relationship between the activation energy and kinetic control steps is presented in Table 6.[28−34]

The apparent activation energy of the leaching process was calculated using the Arrhenius equation, which reveals the temperature dependence on the reaction rate constant (k). The equation used is as follows:

$$k = k_0 \exp[-Ea/(RT)] \quad (12)$$

where k is the reaction rate constant at temperature T, k_0 is the pre-exponential factor, min^{-1}, T is the reaction temperature (K), R is the mole gas constant (8.314 J/(mol·K)), and Ea is the apparent reaction activation energy (J/mol).

According to the Arrhenius equation (eq 12), the plot of $\ln k$ versus $1/T$ was constructed, and the slope for the figure was $-Ea/R$. The results are shown in Figure 18.

From the slope of the fitted equation shown in Figure 18, the activation energy is calculated to be 26.29 kJ/mol. According to the relationship between the activation energy and kinetic control steps (Table 6), the leaching reaction was confirmed to be a mixed control (chemical reaction and diffusion).

3.4.3. Establishment of Kinetics Equation. The effects of the liquid-to-solid ratio and particle size on the reaction kinetics were analyzed using eq 11, and the results are presented in Figure 19a,c, respectively.

A kinetic equation was established to determine the cause of the varied reactions of different liquid-to-solid ratio (L/S), particle sizes (r_0), and temperatures (T) that influenced the leaching efficiency of potassium during the leaching process. This is expressed as follows:

$$k = k_0 (L/S)^a r_0^{\ b} \exp(-Ea/RT) \quad (13)$$

https://doi.org/10.1021/acsomega.3c04733
ACS Omega 2023, 8, 37162−37175

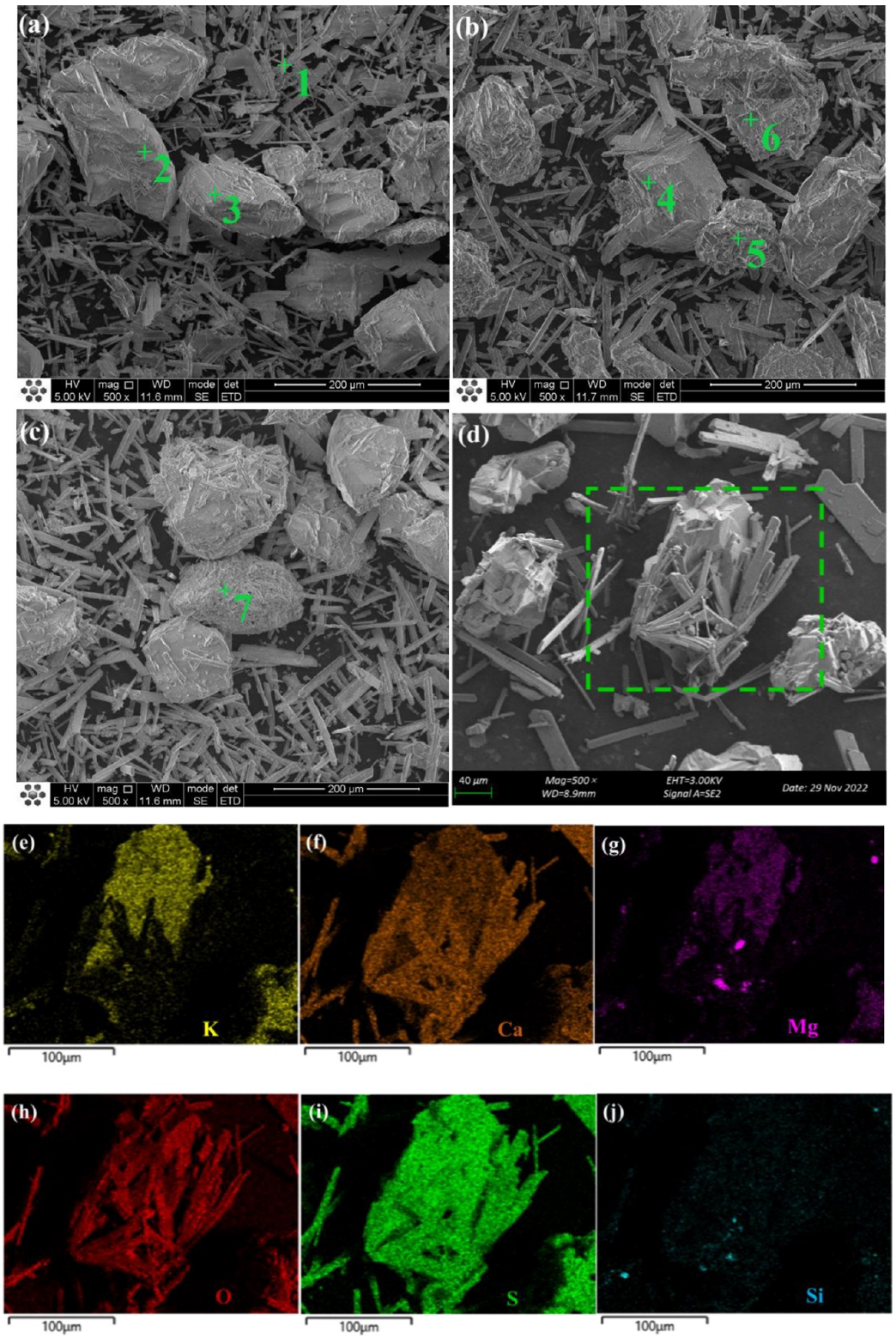

Figure 15. BSE images (a, b, c, d) and elemental mappings (e−j) of residues (Reaction time: 180 min, Particle size: −170 + 125 μm, L/S:10:1 mL/g, Stirring speed: 450 r/min, Temperature: 90 °C).

$$-\ln(1 - x) = k_0(L/S)^a r_0^{\ b} \exp(-Ea/RT)t^n \quad (14)$$

The logarithm is taken on both sides of eq 13 to obtain eq 15.

$$\ln k = \ln k_0 + a \ln(L/S) + b \ln r_0 - \frac{Ea}{RT} \quad (15)$$

where k is the reaction rate constant at temperature T; k_0 is the frequency factor, min^{-1}; a is the reaction order of liquid-to-solid ratio; b is the reaction order of particle sizes; T is the reaction temperature, K; R is the mole gas constant, 8.314 J/(mol·K); and Ea is the apparent reaction activation energy, J/mol.

https://doi.org/10.1021/acsomega.3c04733
ACS Omega 2023, 8, 37162−37175

Table 5. EDS Analysis Results

Position in Figure 15a−c	Elements (wt %)						Main minerals
	K	Ca	Mg	S	O	Si	
1	0.02	23.41	0.24	19.42	56.91	–	Gypsum
2	0.08	23.20	0.64	19.38	56.70	–	Gypsum
3	2.88	24.18	2.09	20.18	50.67	–	Gypsum, Polyhalite
4	5.57	16.29	2.91	17.02	57.66	–	Gypsum, Polyhalite
5	0.40	19.22	1.05	18.27	61.06	–	Gypsum
6	10.65	14.33	4.33	20.49	50.19	–	Polyhalite
7	1.38	31.13	0.67	23.75	43.08	–	Anhydrite, Polyhalite
Mapping	5.47	16.77	2.05	17.92	57.61	0.18	Gypsum, Polyhalite

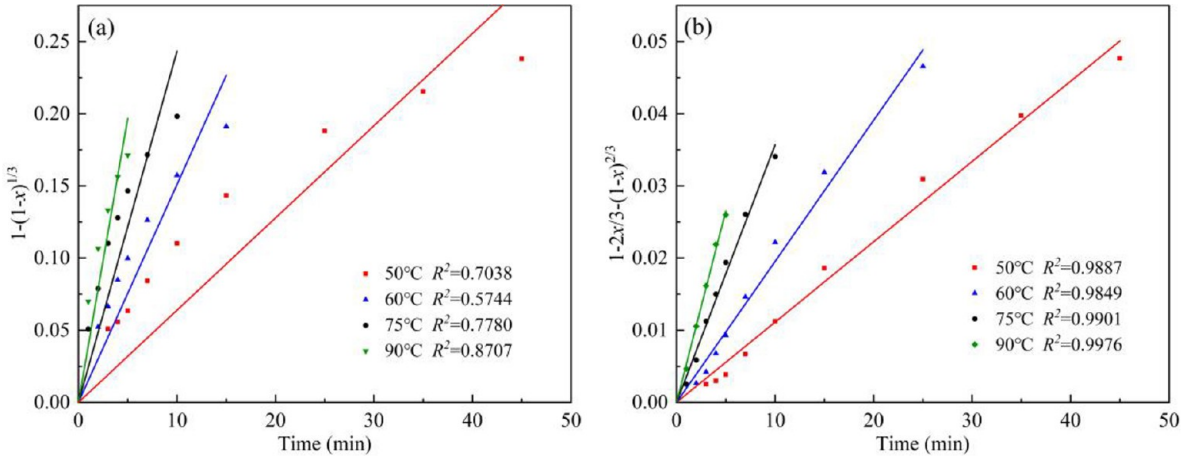

Figure 16. Relationship between $1-(1-x)^{1/3}$ (a), $1-2x/3-(1-x)^{2/3}$ (b), and time at different temperatures

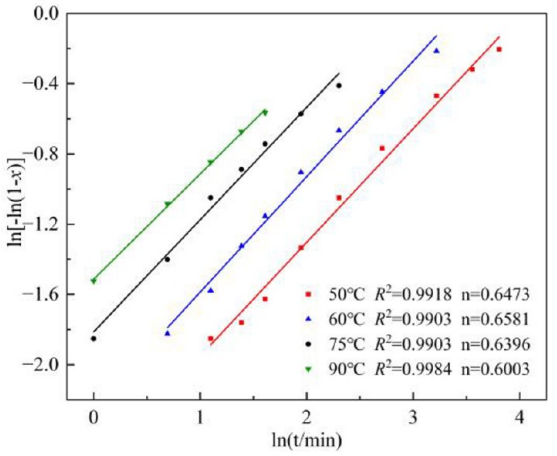

Figure 17. Relationship between $\ln[-\ln(1-x)]$ and $\ln t$ at different reaction temperatures.

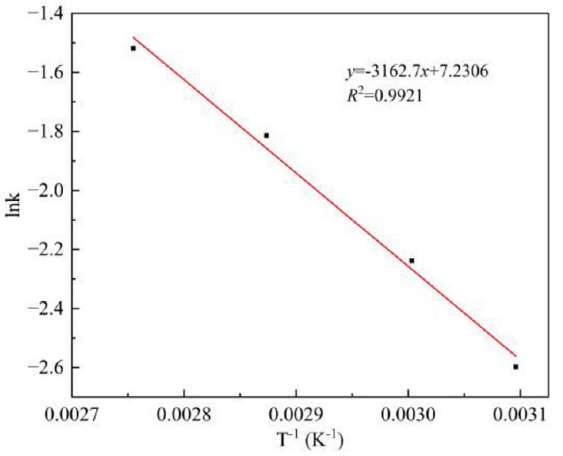

Figure 18. Arrhenius plot of the Avrami model reaction rates for potassium extractions against reciprocal temperature.

Table 6. Kinetic Control Step and Activation Energy

Kinetic control step	Activation energy (kJ·mol^{-1})
Diffusion control	<10, 4−12
Mixed control	10−40, 12−41.8
Chemical reaction control	>40, >41.8, >42

According to eq 15, $\ln k$ is plotted as $\ln(L/S)$ when the leaching agent is an aqueous solution and the temperature and particle sizes are constant, and the result is shown in Figure 19b. Figure 19d shows the results of $\ln k$ plotted against $\ln r_0$ when the leaching agent is an aqueous solution and the temperature and liquid−solid ratio are constant.

a (reaction order of the liquid-to-solid ratio) and b (reaction order of particle sizes) were calculated based on Figure 19b,d and were 0.4452 and −0.2445, respectively. Then the data of a, b, and Ea were substituted into eq 14, and the plot of $-\ln(1-x)$ versus $r_0^{-0.2445}(L/S)^{0.4452}\exp(-26294.69/RT)t^{0.6606}/10^{-3}$ was constructed, and the slope for the figure was $k_0/1000$. The results are listed in Figure 20.

The k_0 calculated from Figure 20 was 1913.90, and the macroscopic leaching kinetic equation of potassium from polyhalite ore in water is

https://doi.org/10.1021/acsomega.3c04733
ACS Omega 2023, 8, 37162−37175

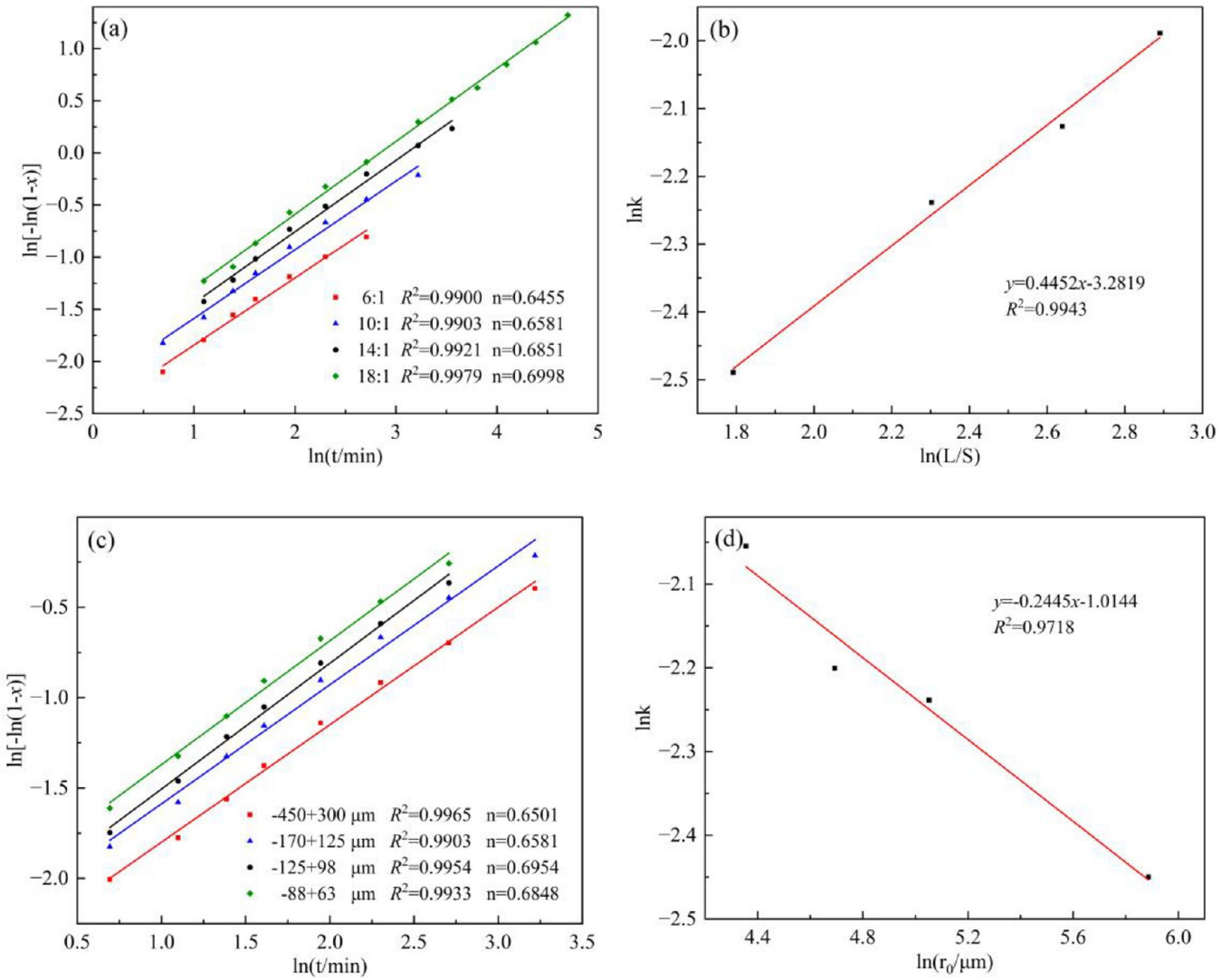

Figure 19. Relationship between $\ln[-\ln(1-x)]$ and $\ln t$ for potassium leaching (a, c); the Arrhenius plots for the leaching kinetics of polyhalite (b, d); (a, b) liquid-to-solid ratio; (c, d) particle size.

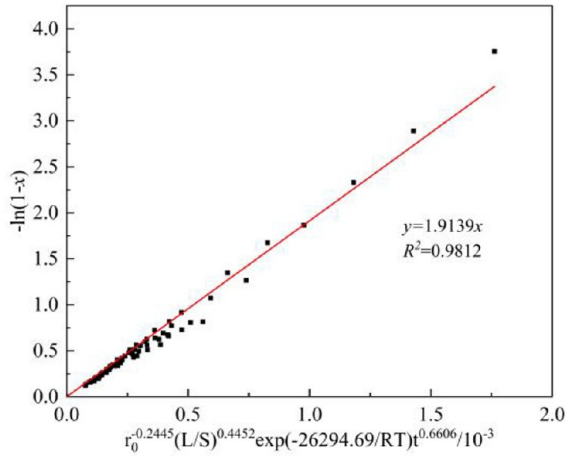

Figure 20. Relationship between $-\ln(1-x)$ and $r_0^{-0.2445}(L/S)^{0.4452}\exp(-26294.69/RT)t^{0.6606}/10^{-3}$.

$$-\ln(1-x) = 1913.9(L/S)^{0.4452} r_0^{-0.2445} \exp(-26294.69/RT)t^{0.6606} \quad (16)$$

3.5. Mechanism Analysis of Polyhalite Ore Leaching Process. According to the K−Mg molar ratio in the leaching solution (Section 3.2.3), the concentration variation of Ca in the leaching solution (Section 3.2.3), and the XRD and SEM-EDS-Mapping analyses of the polyhalite ore before and after leaching (Section 3.3), the leaching mechanisms of K in polyhalite are shown in Figure 21.

It is reasonable to deduce that polyhalite is dissolved and ionized into K^+, Mg^{2+}, Ca^{2+}, and SO_4^{2-} in water. Ca^{2+} reacts with SO_4^{2-} in the liquid phase to form $CaSO_4{\cdot}2H_2O$, which reduces the activity and concentration of Ca^{2+} and SO_4^{2-}, thus

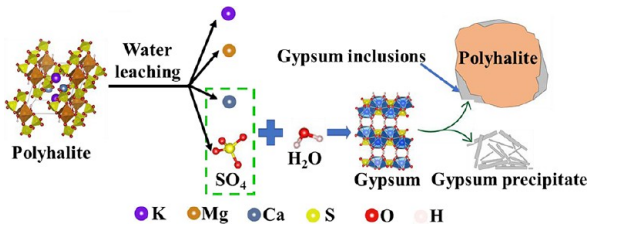

Figure 21. Schematic diagram of the leaching mechanism of the polyhalite in water.

https://doi.org/10.1021/acsomega.3c04733
ACS Omega 2023, 8, 37162−37175

promoting the progress of the leaching reaction. Some $CaSO_4 \cdot 2H_2O$ crystals covered the surfaces of the unreacted polyhalite particles, which probably passivated the polyhalite surface and hindered potassium leaching. Most calcium sulfate exists independently in a crystalline form and constitutes the main component of the leaching residue.

Comprehensive analysis of leaching experiments, characterization of leaching residue, thermodynamics, and kinetics, and the main reasons for hindering the leaching of potassium are listed as follows: (a) the thermodynamic driving force of the leaching reactions of polyhalite with water is small; (b) the solid $CaSO_4 \cdot 2H_2O$ product was coated on the surface of undecomposed polyhalite particles.

NaCl solution could improve the solubility of $CaSO_4 \cdot 2H_2O$, and it also affects the nucleation, crystalline form, and morphology of $CaSO_4 \cdot 2H_2O$.[35] Thus, we can try to using NaCl as a leaching agent to remove the $CaSO_4 \cdot 2H_2O$ product layer wrapped around the outside of undecomposed polyhalite particles to achieve enhanced leaching of K from polyhalite ore.

4. CONCLUSIONS

(1) Leaching experiments indicated that high temperature improves the leaching efficiency at the beginning (1−15 min). With further extension in the leaching time, the leaching efficiency of potassium at 75 °C, 60 °C, and 50 °C gradually exceeded that at 90 °C. When the reaction time was 180 min, the higher the temperature, the lower the efficiency of potassium, which is caused by the fact that temperature rising will reduces the thermodynamic driving force of the leaching reaction.

(2) The XRD, BSE, and EDS analyses of the leaching residue showed that a considerable number of $CaSO_4 \cdot 2H_2O$ crystals were produced during polyhalite leaching. Some $CaSO_4 \cdot 2H_2O$ crystals covered the surfaces of the unreacted polyhalite particles, which may have passivated the polyhalite surface and hindered potassium leaching. These $CaSO_4 \cdot 2H_2O$ inclusions are nondense. In some areas of polyhalite particles, effective contact with the leaching agent can still be established through the pore. Therefore, the leaching reaction can still proceed slowly until equilibrium is reached.

(3) The kinetic analysis shows that the leaching kinetics of potassium are well described by the Avrami model, and the leaching process of potassium from polyhalite ore in water was controlled by a mixed mechanism of surface chemical reaction and diffusion, with an apparent activation energy *Ea* of 26.29 kJ/mol.

(4) Future research will focus on select NaCl as potential "enhance" leaching agent, to achieve green and efficient leaching of K.

AUTHOR INFORMATION

Corresponding Author

Ying Zeng − *College of Materials and Chemistry & Chemical Engineering, Chengdu University of Technology, Chengdu 610059, China;* orcid.org/0000-0002-2797-5559; Email: zengyster@163.com

Authors

Fangtong Ma − *College of Materials and Chemistry & Chemical Engineering, Chengdu University of Technology, Chengdu 610059, China;* orcid.org/0009-0006-3106-0657

Xudong Yu − *College of Materials and Chemistry & Chemical Engineering, Chengdu University of Technology, Chengdu 610059, China;* orcid.org/0000-0002-3848-9484

Ke Chen − *College of Materials and Chemistry & Chemical Engineering, Chengdu University of Technology, Chengdu 610059, China*

Siying Ren − *College of Materials and Chemistry & Chemical Engineering, Chengdu University of Technology, Chengdu 610059, China*

Complete contact information is available at: https://pubs.acs.org/10.1021/acsomega.3c04733

Notes

The authors declare no competing financial interest.

ACKNOWLEDGMENTS

The authors are grateful to the National Natural Science Foundation of China (No. U21A2017).

REFERENCES

(1) Johnson, R.; Vishwakarma, K.; Hossen, M. S.; Kumar, V.; Shackira, A.M.; Puthur, J. T.; Abdi, G.; Sarraf, M.; Hasanuzzaman, M. Potassium in plants: Growth regulation, signaling, and environmental stress tolerance. *Plant Physiol. Biochem.* **2022**, *172*, 56−69.

(2) Song, X.; Geng, Y.; Zhang, Y.; Zhang, X.; Gao, Z.; Li, M. Dynamic potassium flows analysis in China for 2010−2019. *J. Resour. Policy* **2022**, *78*, 102803.

(3) Ma, J.; Du, X.; Qin, Y.; Wu, Z.; Chi, R.; Wang, C. Kinetics on leaching of potassium from phosphorus-potassium associated ore in HCl-H_3PO_4 media. *Trans. Nonferrous Met. Soc. China* **2017**, *27* (8), 1870−1877.

(4) Zheng, M.; Zhang, Y.; Shang, W.; Xing, E.; Zhong, J.; Gui, B.; Peng, Y. Discovery of a new type of polyhalite potassium ore in Puguang region, northeastern Sichuan. *Geol. China* **2018**, *45* (5), 1074−1075.

(5) Weck, P. F.; Kim, E.; Jove-colon, C. F.; Sassani, D. C. First-principles study of anhydrite, polyhalite and carnallite. *Chem. Phys. Lett.* **2014**, *594*, 1−5.

(6) Xu, H.; Guo, X.; Bai, J. Thermal behavior of polyhalite: a high-temperature synchrotron XRD study. *Phys. Chem.Miner.* **2017**, *44* (2), 125−135.

(7) Tan, H.; Cui, Y.; Liu, C.; Zeng, F.; Han, C.; Zhang, H.; Fan, X.; Mitchell, R.; Yan, D.; Zhang, D. Toward the replacement of conventional fertilizer with polyhalite in eastern China to improve peanut growth and soil quality. *Chem. Biol. Technol. Agric.* **2022**, *9* (1), 1−17.

(8) Li, R.; Liu, C.; Jiao, P.; Liu, W.; Tang, D.; Wang, S. The effect of solvent chemistry on potassium dissolution extraction from low-grade solid potash ore in Qarhan Salt Lake. *China. J. Appl. Geochem.* **2020**, *115*, 104550.

(9) Zhou, T.; Cheng, H.; Zhang, X.; Du, Y.; Li, Y.; Wan, W. Study on the Dissolution Difference of Polyhalite Ore in Modern Salt Lake by Inorganic Salts Leaching Agents. *J. Salt Lake Res.* **2020**, *28* (04), 71−78.

(10) Tanaydin, M. K.; Tanaydin, Z. B.; Demirkiran, N. Optimization of process parameters and kinetic modelling for leaching of copper from oxidized copper ore in nitric acid solutions. *Trans. Nonferrous Met. Soc. China* **2022**, *32* (4), 1301−1313.

(11) Luo, Y.; Chen, X.; Zhao, Z.; Liu, X.; Li, J.; He, L.; Sun, F. Pressure leaching of wolframite using a sulfuric-phosphoric acid mixture. *Miner. Eng.* **2021**, *169*, 106941.

(12) Petrovic, S. J.; Bogdanovic, G. D.; Antonijevic, M. M. Leaching of chalcopyrite with hydrogen peroxide in hydrochloric acid solution. *Trans. Nonferrous Met. Soc. China* **2018**, *28* (7), 1444−1455.

(13) Xu, Y.; Xia, H.; Zhang, Q.; Cai, W.; Jiang, G.; Zhang, L. Efficient recovery of valuable metals from lead-zinc smelting by-products by ultrasonic strengthening. *Miner. Eng.* **2022**, *190*, 107915.

(14) Li, J.; Yang, J.; Zhao, Z.; Chen, X.; Liu, X.; He, L.; Sun, F. Efficient extraction of tungsten, calcium, and phosphorus from low-grade scheelite concentrate. *Miner. Eng.* **2022**, *181*, 107462.

(15) Duan, W.; Wang, D.; Wang, Z.; Zhan, Y.; Mu, T.; Yu, Q. A novel synergistic method on potential green and high value-added utilization of blast furnace slag. *J. Cleaner Prod.* **2021**, *329*, 129804.
(16) Ogorodova, L. P.; Vigasina, M. F.; Mel'chakova, L. V.; Bryzgalov, I. A.; Ksenofontov, D. A. Enthalpy of formation of natural polyhalite. *Geochem. Int.* **2016**, *54*, 645−649.
(17) Wagman, D. D.; Evans, W. H.; Parker, V. B.; Schumm, R. H.; Halow, I.; Bailey, S. M.; Churney, K. L.; Nuttall, R. L. The NBS tables of chemical thermodynamic properties. Selected values for inorganic and C_1 and C_2 organic substances in SI units. *J. Phys. Chem. Ref. Data* **1982**, *11*, 1−392.
(18) Shock, E. L.; Helgeson, H. C. Calculation of thermodynamic and transport properties of aqueous species at high pressures and temperatures: correlation algorithms for ionic species and equation of state predictions to 5 kbar and 1000 °C. *Geochim. Cosmochim. Acta* **1988**, *52* (8), 2009−2036.
(19) Tumen-ulzii, N.; Batnasan, A.; Gunchin, B. Selective dissolution of copper and iron from molybdenite concentrate using acidic sodium nitrate solution. *Miner. Eng.* **2022**, *185*, 107715.
(20) Zhu, X.; Xiao, J.; Mao, Q.; Zhang, Z.; You, Z.; Tang, L.; Zhong, Q. A promising regeneration of waste carbon residue from spent Lithium-ion batteries via low-temperature fluorination roasting and water leaching. *Chem. Eng. J.* **2022**, *430*, 132703.
(21) Li, D.; Gao, D.; Bian, S.; Li, W.; Dong, Y. Revisiting the crystallization field of polyhalite in the six-component system Na^+, K^+, Mg^{2+}, Ca^{2+}// Cl^-, SO_4^{2-} H_2O. *J. Earth Sci. Front.* **2021**, *28* (06), 46−55.
(22) Levenspiel, O. *Chemical reaction engineering*; 3rd ed.; John Wiley & Sons: New York, NY, USA, 1998.
(23) Du, H.; Wang, D.; Zhang, L.; Li, W.; Wang, Z.; Xiao, W.; Ye, C. Extraction of rare earth and cobalt from leach residue of Nd-Fe-B waste by reductive leaching with iron powder. *Hydrometallurgy* **2022**, *213*, 105942.
(24) Avrami, M. Kinetics of Phase Change. I General Theory. *J. Chem. Phys.* **1939**, *7* (12), 1103−1112.
(25) Avrami, M. Granulation, phase change, and microstructure: Kinetics of phase change. III. *J. Chem. Phys.* **1941**, *9* (2), 177−184.
(26) Yang, Q.; Li, Q.; Zhang, G.; Shi, Q.; Feng, H. Investigation of leaching kinetics of aluminum extraction from secondary aluminum dross with use of hydrochloric acid. *Hydrometallurgy* **2019**, *187*, 158−167.
(27) Li, Y.; Cheng, H.; Gong, P.; Yang, K.; Tian, Z.; Lai, Y. An environmentally benign and sustainable process for carbon recovery and efficient defluorination of spent carbon cathode. *Trans. Nonferrous Met. Soc. China* **2022**, *32* (11), 3810−3821.
(28) Guo, X.; Xin, Y.; Wang, H.; Tian, Q. Mineralogical characterization and pretreatment for antimony extraction by ozone of antimony-bearing refractory gold concentrates. *Trans. Nonferrous Met. Soc. China* **2017**, *27* (8), 1888−1895.
(29) Zhang, X.; Cao, H.; Xie, Y.; Ning, P.; An, H.; You, H.; Nawaz, F. A closed-loop process for recycling $LiNi_{1/3}Co_{1/3}Mn_{1/3}O_2$ from the cathode scraps of lithium-ion batteries: Process optimization and kinetics analysis. *Sep. Purif. Technol.* **2015**, *150*, 186−195.
(30) Wu, J.; Xiao, Y.; Yang, X.; Xu, D.; Zhang, Z.; Zhong, Y.; Wang, X. Leaching kinetics for magnesium extraction from phosphate rock in the nitric acid method. *Miner. Eng.* **2022**, *189*, 107894.
(31) Lou, W.; Zhang, Y.; Zhang, Y.; Zheng, S.; Sun, P.; Wang, X.; et al. Leaching performance of Al-bearing spent $LiFePO_4$ cathode powder in H_2SO_4 aqueous solution. *Trans. Nonferrous Met. Soc. China* **2021**, *31* (3), 817−831.
(32) Han, J.; Wang, Y.; Mao, X.; Chang, X.; Zeng, H.; Qin, W. Efficient extraction of nickel from sintered alloy by stepwise leaching: Thermodynamic and kinetic studies. *Miner. Eng.* **2022**, *187*, 107776.
(33) Tian, Y.; Quan, X.; Li, G.; Tang, X.; Qin, X.; Wu, H.; Zeng, K.; Jiang, Z. A cleaner method for preparation of chromium oxide from chromite ore. *Process Saf. Environ. Prot.* **2022**, *158*, 87−97.
(34) Habashi, F. *Principles of Extractive Metallurgy*, 2nd ed.; Gordon and Breach: New York, 1980.
(35) Ben Ahmed, S.; Tlili, M. M.; Amami, M.; Ben Amor, M. Gypsum Precipitation Kinetics and Solubility in the $NaCl$-$MgCl_2$-$CaSO_4$-H_2O System. *Ind. Eng. Chem. Res.* **2014**, *53* (23), 9554−9560.

https://doi.org/10.1021/acsomega.3c04733
ACS Omega 2023, 8, 37162−37175